

Article

# Corrosion Behavior of SMA490BW Steel and Welded Joints for High-Speed Trains in Atmospheric Environments

Xiangyang Wu <sup>1</sup>, Zhiyi Zhang <sup>1</sup>, Weichuang Qi <sup>1</sup>, Renyong Tian <sup>1</sup>, Shiming Huang <sup>2,\*</sup> and Chunyuan Shi <sup>2</sup>

<sup>1</sup> CRRC Sifang Co. Ltd., Qingdao 266111, China; sfxiangyangw@163.com (X.W.); yefan0954@163.com (Z.Z.); qwc5137@163.com (W.Q.); tianrenyonghj@163.com (R.T.)

<sup>2</sup> School of Materials Science and Engineering, Dalian Jiaotong University, Dalian 116028, China; shicy@sina.com

\* Correspondence: huangsm@djtu.edu.cn

Received: 22 August 2019; Accepted: 17 September 2019; Published: 19 September 2019



**Abstract:** Currently, high-speed trains work under various atmospheric environments, and the bogie as a key component suffers serious corrosion. To investigate the corrosion behavior of bogies in industrial atmospheric environments, the periodic immersion wet/dry cyclic corrosion test for SMA490BW steel and automatic metal active gas (MAG) welded joints used for bogies was conducted in the present work. Corrosion weight loss rate, structure, and composition of rust layers as well as electrochemistry parameters were investigated. The results showed that the corrosion weight loss rate decreased with increasing corrosion time; furthermore, the corrosion weight loss rate of the welded joints was lower than that of SMA490BW steel. The XRD results showed that the rust layers formed on SMA490BW steel and its welded joints were mainly composed of  $\alpha$ -FeOOH,  $\gamma$ -FeOOH, Fe<sub>2</sub>O<sub>3</sub>, and Fe<sub>3</sub>O<sub>4</sub>. The observation of surface morphology indicated that the rust layers of the welded joints were much denser and had a much finer microstructure compared with those of SMA490BW steel. After corrosion for 150 h, the corrosion potential of the welded joints with rust layers was higher than that of SMA490BW steel. In short, the welded joints exhibited better corrosion resistance than SMA490BW steel because of the higher content of alloy elements, as shown in this work.

**Keywords:** bogie; SMA490BW; corrosion behavior; atmospheric environment; corrosion weight loss rate; potentiodynamic polarization curve

## 1. Introduction

The bogie, as one of the key components of high-speed trains, operates with the functions of load bearing, guidance, and propulsion, and its performance affects the running quality and security of high-speed trains directly [1,2]. High-speed trains work under various atmospheric environments, and the bogie's surface suffers different degrees of corrosion. A corrosion status survey of high-speed trains in commission showed that the bogie was affected by serious corrosion, and that the corrosion reaction would continue in a corrosive environment [3–5]. More importantly, the bogie's bearing strength is reduced due to the corrosion of the bogie, especially of its welded joints. This can lead to a decrease in the bogie's fatigue life. Thus, the study of the corrosion behavior of a bogie and its welded joints has the greatest significance for the safe reliability of high-speed trains.

Weathering steel can be used for the bogies of high-speed trains. Cheng et al. [6] investigated the influence of Ni on the corrosion behavior of Q415NH weathering steel by simulating a marine atmosphere, and found that the addition of Ni not only resulted in a positive shift in corrosion potentials but was also helpful in enhancing corrosion resistance. The research suggested that MnCuP weathering

steel exhibited high corrosion resistance in simulated coastal, industrial, and coastal-industrial atmospheric environments [7]. Zhu et al. investigated the corrosion mechanism of weathering steel in a simulated industrial atmosphere, and found that the non-metallic oxide affected corrosion resistance [8]. So far, most of the previous studies have focused on the corrosion behavior of these types of steel in different atmospheric environments, and yet there are few reports dealing with the materials used for high-speed train bogies, such as SMA490BW steel [9]. Moreover, the difference in the corrosion behavior between SMA490BW steel and its welded joints is still not clearly understood. In the present work, the corrosion behavior of SMA490BW steel and its welded joints, which are used for high-speed train bogies in China, was investigated using the periodic immersion wet/dry cyclic corrosion test to simulate an industrial atmospheric environment. In order to analyze the corrosion mechanism, corrosion weight loss rate, structure, and composition of rust layers as well as the potentiodynamic polarization curve were also investigated. This provides essential data for the safe reliability of bogies found in high-speed trains in commission.

## 2. Materials and Methods

### 2.1. Materials

The raw material used was SMA490BW steel plate with dimensions of 350 × 150 × 12 mm (length × width × thickness). The welding wire was CHW-55CNH (Sichuan Atlantic Co. Ltd., Zigong, China) with a diameter of 1.2 mm. The shield gas was a mixed gas of 80% argon and 20% carbon dioxide. The chemical compositions of SMA490BW steel and CHW-55CNH welding wire are given in Table 1.

**Table 1.** Chemical composition of experimental materials (wt %).

Materials	C	Si	Mn	S	P	Cu	Cr	Ni	Fe
SMA490BW	≤0.18	0.15–0.65	≤1.40	≤0.005	≤0.035	0.30–0.50	0.45–0.75	0.08–0.25	Bal.
CHW-55CNH	≤0.10	0.35–0.65	1.20–1.60	≤0.025	≤0.025	0.20–0.50	0.30–0.90	0.20–0.60	Bal.

### 2.2. Methods

The SMA490BW steel was polished with abrasive papers, and then cleaned with acetone before welding. The butt joints of SMA490BW steel were prepared by single-wire automatic metal active gas (MAG) arc welding with a TPS5000 welding machine (Fronius Intelligent Equipment China Co. Ltd., Zhuhai, China). The groove type was V-groove with a bevel angle of 60°, and the root face dimension was 1 mm. The process parameters of multipass welding are given in Table 2.

**Table 2.** Welding process parameters.

Number of Weld Passes	Welding Current (I)/A	Arc Voltage (U)/V	Welding Speed (v)/(mm·s <sup>-1</sup> )	Welding Heat Input (E)/(kJ·cm <sup>-1</sup> )
1	240	25	8.3	4.3
2–4	245–250	27	5.0–8.3	6.4

The periodic immersion wet/dry cyclic corrosion test for SMA490BW steel and its welded joints was carried out on an FL-65 testing machine (Zhongfeijingchi Co. Ltd., Beijing, China) according to ISO 11330: 1999. To simulate an industrial atmospheric environment, the corrosion solution used was NaHSO<sub>3</sub> with an initial concentration of  $(1.0 \pm 0.05) \times 10^{-2}$  mol/L (pH 4.4) and the replenisher was NaHSO<sub>3</sub> with an initial concentration of  $(2.0 \pm 0.05) \times 10^{-2}$  mol/L. The specimen size was 60 × 40 × 4 mm as shown in Figure 1.

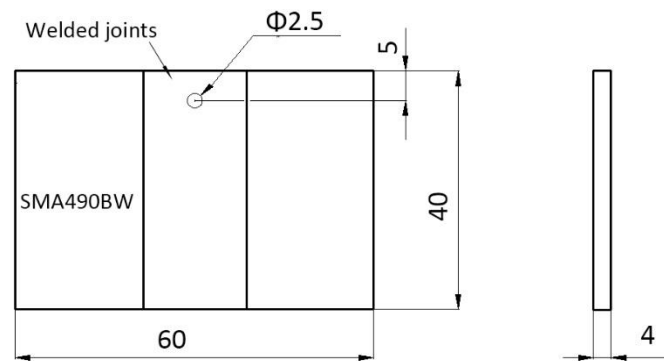


Figure 1. Specimen for the periodic immersion wet/dry cyclic corrosion test.

First, the specimens were polished by abrasive papers to remove the oxide layer, and then cleaned by means of ultrasonic cleaning with petroleum ether, anhydrous alcohol, and acetone. Second, the initial weight of the specimens after being put in a dryer for 24 h was obtained by electronic scales with an accuracy of 0.1 mg. Third, 25 specimens for each material were put in the testing machine, ready for testing. Each wet/dry cycle test lasted 1 h and contained two stages: (1) the specimens were immersed in  $\text{NaHSO}_3$  (pH 4.4) at a temperature of 45 °C for 12 min; and (2) the specimens were hung and dried at 70% relative humidity for 48 min, and the specimen's surface temperature was no more than 70 °C. The test period lasted 50 h, 75 h, 100 h, 125 h, and 150 h, respectively. For each material, five specimens were brought out after each test period, and one of them was used for microstructure and phase analysis. The others were rinsed with a HCl solution with hexamethylene tetramine to remove corrosion products, and subsequently washed with distilled water, anhydrous alcohol, and acetone. Then, the specimens were dried for 24 h and weighed.

The corrosion weight loss rate was calculated using the following equation [10]:

$$W = \frac{m_0 - m_1}{2(a \times b + b \times c + a \times c)t} \times 10^6, \quad (1)$$

where  $W$  is the corrosion weight loss rate ( $\text{g}/\text{m}^2 \cdot \text{h}$ ),  $m_0$  is the initial weight of the specimens (g),  $m_1$  is the weight of the specimens after the corrosion test (g),  $a$ ,  $b$ , and  $c$  are the length, width, and thickness of the specimens, respectively, and  $t$  is the corrosion time (h).

The phase composition of the rust layers formed on the specimens after the corrosion test was identified by X-ray diffraction analysis (XRD, Empyrean-X, Almelo, Holland) with  $\text{Cu-K}\alpha$  radiation operated at 50 kV and 40 mA with a scanning speed of  $2^\circ/\text{min}$ . The surface morphology of the rust layers was observed using a field-emission scanning electron microscope (SEM, Supra 55, Shanghai, China).

The electrochemical test was carried out in a 0.01 mol/L  $\text{NaHSO}_3$  (pH 4.4) electrolyte solution on a CHI600B electrochemical workstation (Shanghai Chenhua instrument Co. Ltd., Shanghai, China) at room temperature. A three-electrode system was adopted, namely, a saturated calomel electrode (SCE) as reference electrode, a Pt electrode as auxiliary electrode, and the specimens with rust layers after the wet/dry cyclic corrosion test as working electrode. The sweeping speed for the potentiodynamic polarization curve was 0.33 mV/s [11].

### 3. Results and Discussion

#### 3.1. Corrosion Kinetics

The corrosion weight loss rate of SMA490BW steel and its welded joints in the periodic immersion wet/dry cyclic corrosion test simulating an industrial atmospheric environment was obtained by calculation using Equation (1), and the data are given in Table 3. As shown, a similar pattern was found on SMA490BW steel and its welded joints. The corrosion weight loss rate of SMA490BW steel

and its welded joints increased before 75 h and then decreased with increasing corrosion time. In other words, the corrosion process of SMA490BW steel and its welded joints can be divided into two periods, namely, an accelerated corrosion period (before 75 h) and a stable corrosion period (after 75 h). This can be attributed to the change of surface corrosion products during the corrosion process.

Table 3. Corrosion weight loss of the specimens.

Material	Corrosion Rate of Weight Loss (W)/(g·m <sup>-2</sup> ·h <sup>-1</sup> )				
	50 h	75 h	100 h	125 h	150 h
SMA490BW	3.3212	3.6792	3.1943	2.6497	2.2619
Welded joint	3.0149	3.1862	2.9217	2.5361	2.2175

The corrosion kinetics of steel in atmospheric environment is in accordance with the traditional equation [12] as follows:

$$W = Ct^n, \tag{2}$$

where  $W$  is the corrosion weight loss rate,  $t$  is the corrosion time, and  $C$  and  $n$  are constants. The increase in the corrosion weight loss rate in the accelerated corrosion period (before 75 h) can be attributed to surface toughness and work hardening of the specimens, and the specimens' rust layers did not seem to have a protective capability [13]. Therefore, we only chose the corrosion weight loss rate after 75 h for data fitting in order to verify whether the corrosion kinetics curve was in accordance with Equation (2). Figure 2 shows the fitting curve of the specimens' corrosion weight loss rate. It can be seen that both correlation coefficients  $R^2$  are greater than 0.93, which demonstrates that the corrosion behavior of SMA490BW steel and its welded joints should conform to Equation (2). In addition,  $n < 1$  means that the corrosion weight loss rate decreases with increasing corrosion time; in other words, the rust layers have a good effect on protecting the substrate. Moreover, the corrosion weight loss rate of the welded joints is lower than that of SMA490BW steel. It can be concluded that the corrosion resistance of the welded joints is higher than that of SMA490BW steel in a simulated industrial atmospheric environment.

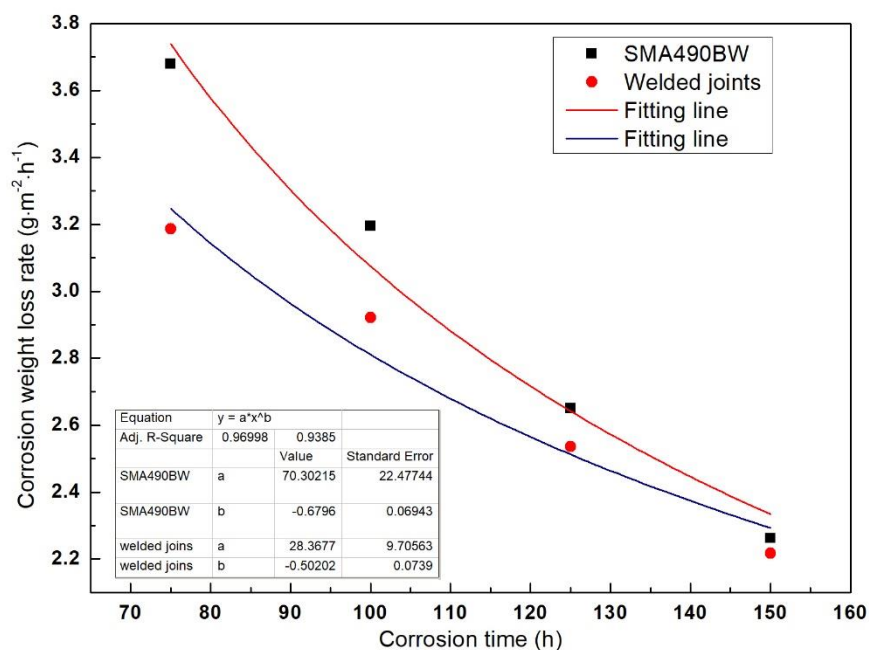
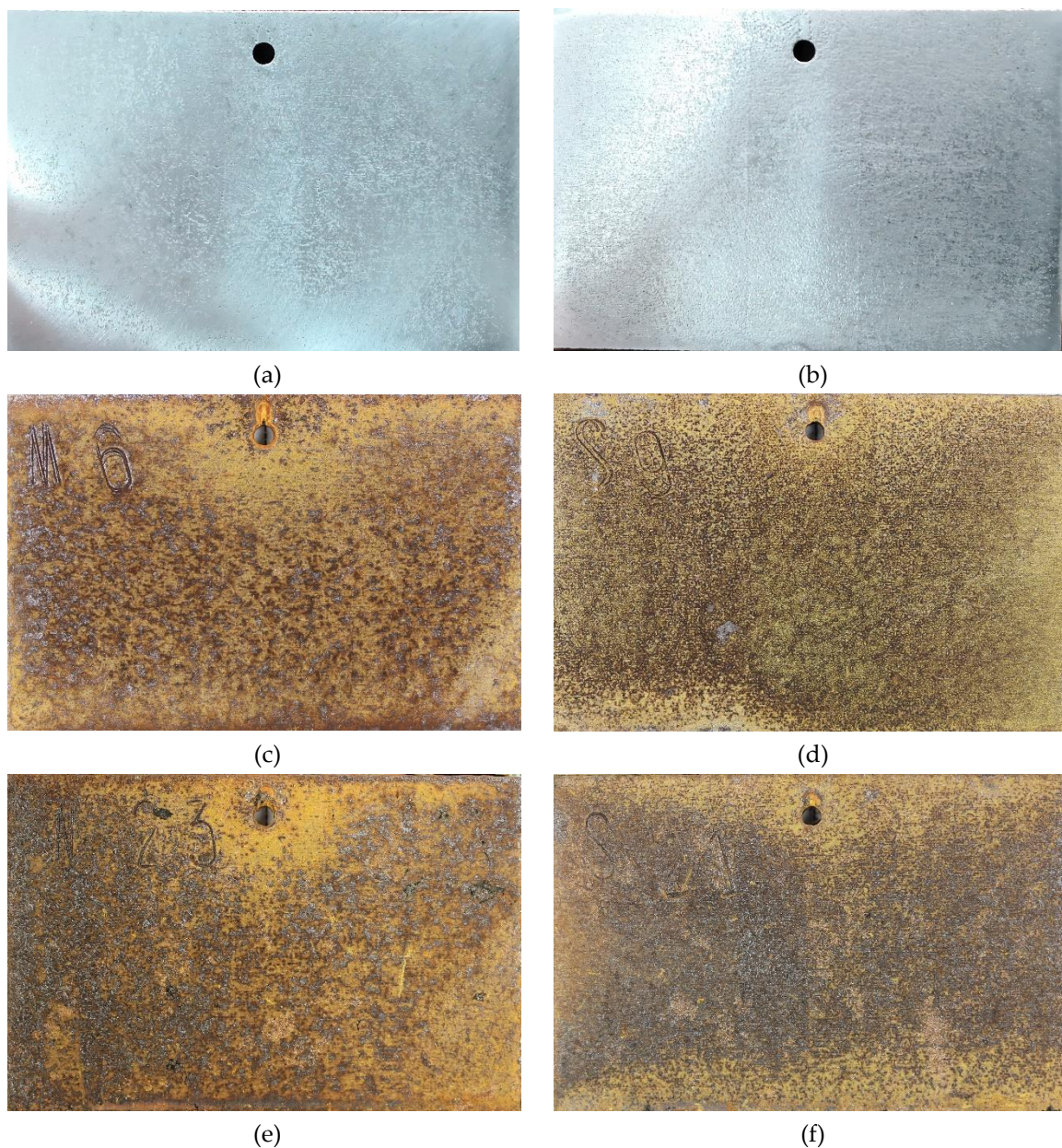


Figure 2. Fitting curve of the specimen's corrosion weight loss rate as a function of corrosion time.

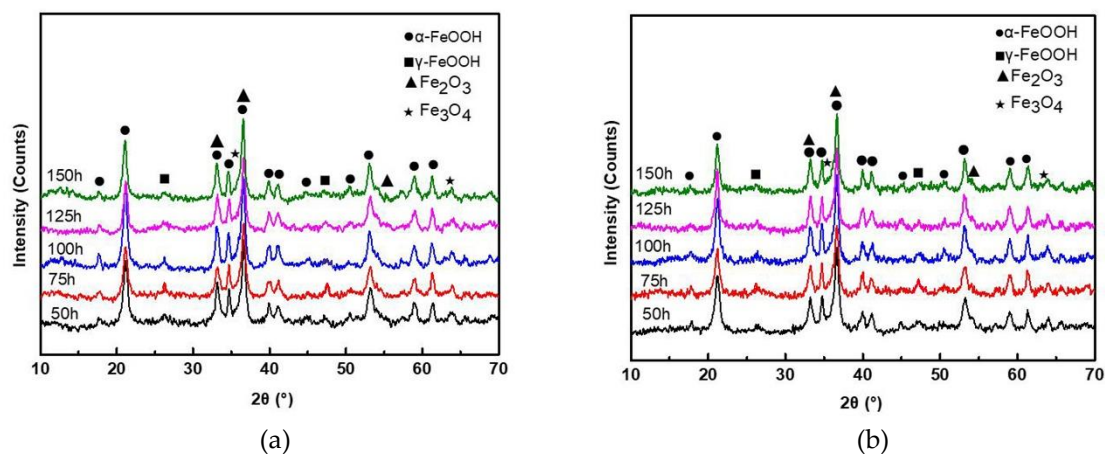
### 3.2. Surface Morphology and Phase Analysis of Rust Layers

Figure 3 shows the surface morphology of SMA490BW steel and its welded joints after the periodic immersion wet/dry cyclic corrosion test. Obviously, the surface morphology of SMA490BW steel is similar to that of its welded joints. There exists a tawny rust layer on the surface, and a black rust layer is compact and adherent to the substrate [14,15]. Compared with the rust layers of the welded joints after 75 h, the rust layers after 150 h are more compact to the benefit of protecting the substrate and inhibiting the mass transfer process of the corrosion solution. This may explain why the corrosion weight loss rate increased first and then decreased with increasing corrosion time. Furthermore, SMA490BW steel had a looser rust layer in comparison with its welded joints at the same corrosion time, meaning that SMA490BW steel suffered more serious corrosion. These results are in agreement with the corrosion weight loss rate in Table 3.



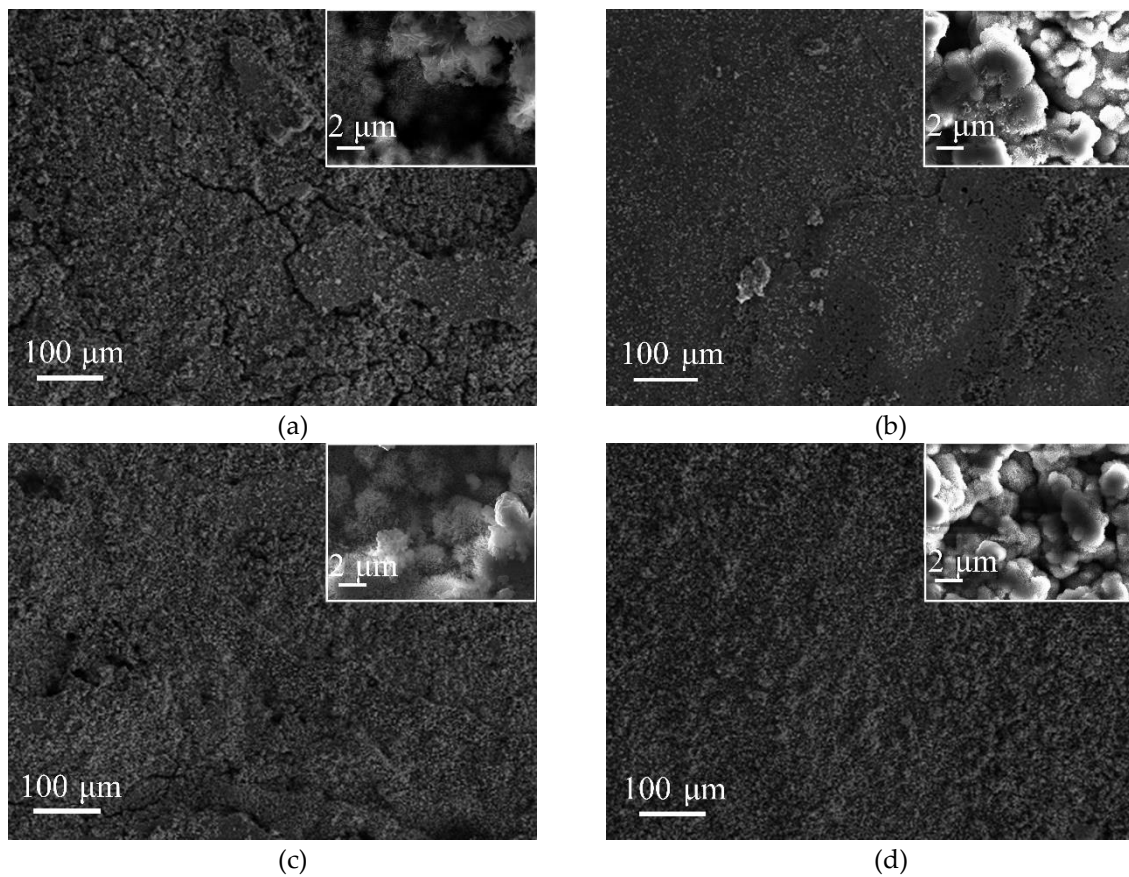
**Figure 3.** Surface morphology of SMA490BW steel (a) as prepared, (c) at 75 h, (e) at 150 h, and welded joints (b) as prepared, (d) at 75 h, (f) at 150 h, after the periodic immersion wet/dry cyclic corrosion test.

The XRD patterns of rust layers formed on SMA490BW steel and its welded joints after the periodic immersion wet/dry cyclic corrosion test are shown in Figure 4. It can be seen that the phase compositions of rust layers formed on SMA490BW steel and its welded joints are quite similar. As shown, the rust layers are mainly composed of  $\alpha$ -FeOOH,  $\gamma$ -FeOOH,  $\text{Fe}_2\text{O}_3$ , and  $\text{Fe}_3\text{O}_4$ . In both the rust layers of SMA490BW steel and its welded joints, the diffraction peaks of  $\gamma$ -FeOOH after 150 h are much weaker than those after 75 h. In contrast, the diffraction peaks of  $\alpha$ -FeOOH are more intensive after 150 h. To some extent, the XRD results suggest that there exists a transform from porous  $\gamma$ -FeOOH to compact  $\alpha$ -FeOOH during the corrosion process [16]. Much research shows that  $\gamma$ -FeOOH is formed from the crystallization of amorphous oxide in the preliminary stage of corrosion and then is partially transformed to  $\alpha$ -FeOOH [17–20]. Furthermore, the volume change due to the phase transformation of  $\gamma$ -FeOOH results in defects in the rust layers, such as pores and cracks. However,  $\alpha$ -FeOOH is a stable oxyhydroxide with no phase transformation in the rust layers so that compact and stable rust layers are formed in favor of protecting the substrate. As shown in Figure 4, the diffraction peaks of  $\alpha$ -FeOOH of the welded joints are more intensive than that of SMA490BW steel; therefore, the welded joints have a better corrosion resistance than SMA490BW steel.



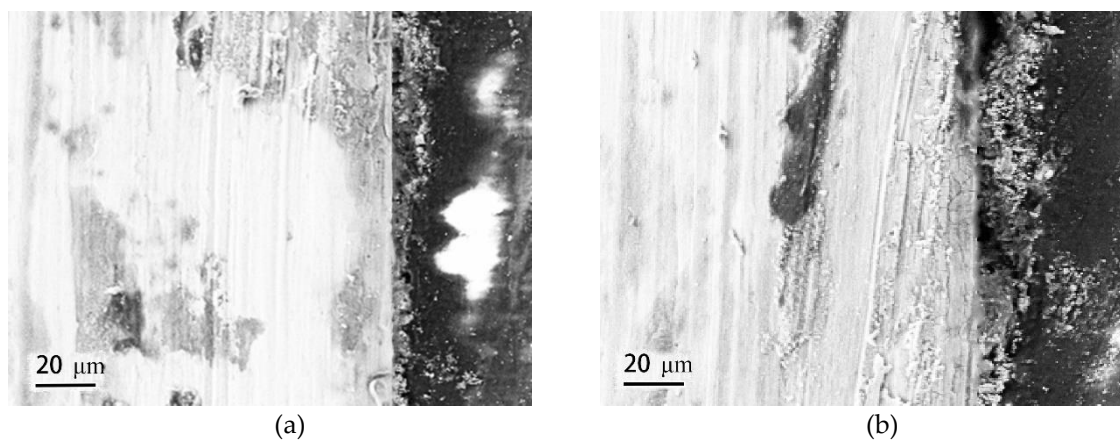
**Figure 4.** XRD patterns of rust layers formed on (a) SMA490BW steel and (b) welded joints after the periodic immersion wet/dry cyclic corrosion test.

Figure 5 presents SEM micrographs of the surface rust layers of SMA490BW steel and its welded joints after the periodic immersion wet/dry cyclic corrosion test. As shown in Figure 5c, it can be seen that the surface rust layers of the welded joints after 75 h are relatively flat. At the same time, however, a thin layer with small cracks and pores is observed. From the inset in Figure 5c with high magnification, the rust layers consist of flower-like  $\gamma$ -FeOOH and spherical  $\alpha$ -FeOOH [21,22]. As shown in Figure 5a, there are more  $\gamma$ -FeOOH and cracks in the rust layers of SMA490BW steel compared with its welded joints. The loose rust layers with porous  $\gamma$ -FeOOH and cracks have no ability to protect the substrate because the porous  $\gamma$ -FeOOH and cracks offer a channel where the corrosion solution can easily invade. Figure 5b,d shows SEM micrographs of the surface rust layers of SMA490BW steel and its welded joints after 150 h, respectively. Although  $\alpha$ -FeOOH and  $\gamma$ -FeOOH can be still observed in the rust layers, it is clear that the rust layers of the welded joints after 150 h became much denser than those of SMA490BW steel. It is known that the protective capability of rust layers depends on the compactness and adherence of rust layers formed on the substrate. Consequently, amounts of  $\alpha$ -FeOOH and compact inner rust layers in the welded joints provide relatively better protection to the substrate [23]. In other words, the welded joints have a better corrosion resistance than SMA490BW steel under this experimental condition, which is consistent with the corrosion weight loss rate and XRD results presented above.



**Figure 5.** SEM micrographs of the surface rust layers of SMA490BW steel (a) 75 h, (b) 150 h, and welded joints (c) 75 h, (d) 150 h, after the periodic immersion wet/dry cyclic corrosion test.

Figure 6 gives the cross-sectional morphologies of SMA490BW steel and its welded joints after the periodic immersion wet/dry cyclic corrosion test. As shown, the rust layers of SMA490BW steel and its welded joints after 75 h are thinner and have many cracks. In contrast, the rust layers after 150 h are more compact and more adherent to the substrate. Furthermore, the rust layers of the welded joints are much thicker and more uniform than that of SMA490BW steel. EDS results of the rust layers indicated that alloy elements, such as Ni and Cr, formed in the rust layers after the periodic immersion wet/dry cyclic corrosion test for 150 h.



**Figure 6.** Cont.

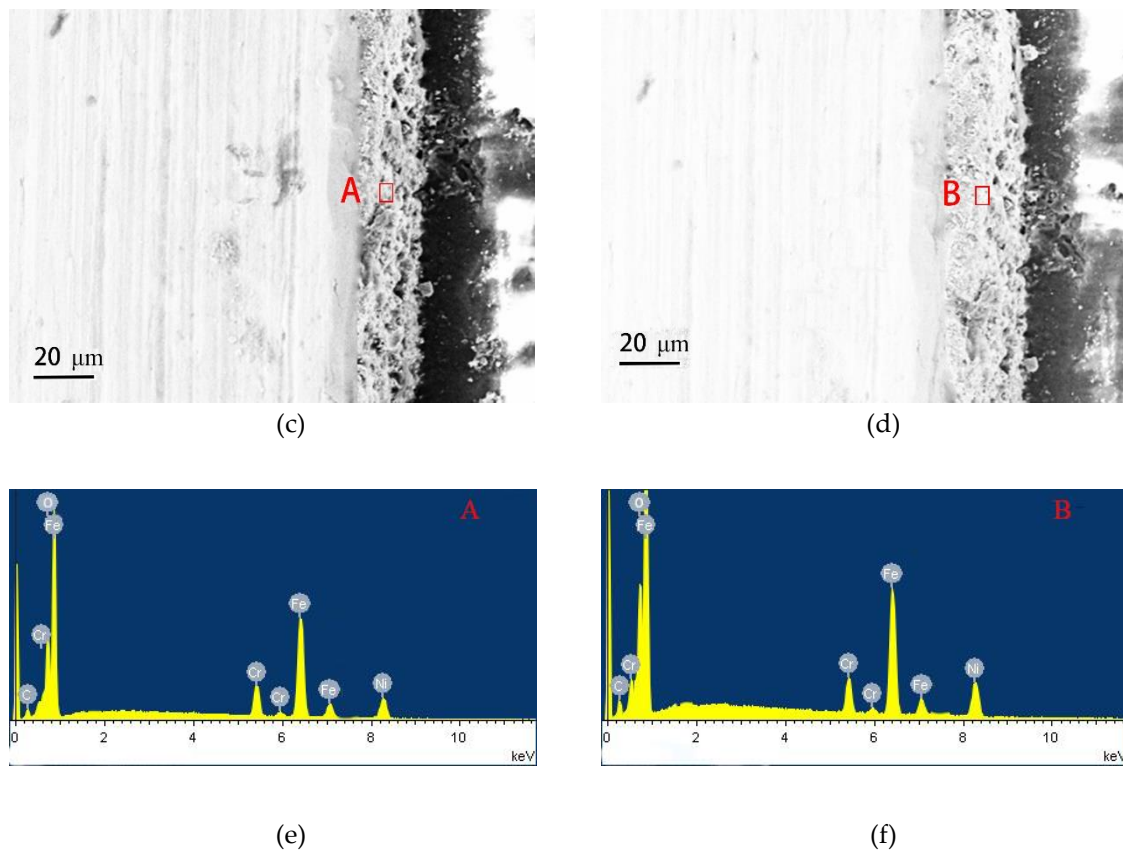


**Figure 6.** Cross-sectional morphologies of SMA490BW steel (a) 75 h, (c) 150 h, and (e) EDS and welded joints (b) 75 h, (d) 150 h, and (f) EDS after the periodic immersion wet/dry cyclic corrosion test.

### 3.3. Electrochemical Test

Figure 7 is the potentiodynamic polarization curve of the specimens with rust layers after the periodic immersion wet/dry cyclic corrosion test. Electrochemical parameters obtained from the polarization curve of SMA490BW steel and its welded joints are given in Table 4. As shown, there is no significant passivation for all the specimens. Moreover, it is obvious that the corrosion potential increases and the corrosion current density decreases with increasing corrosion time, which means that the corrosion rust layers became thicker so that the anodic reaction was restrained by the thick and compact rust layers [24,25]. After 150 h, the welded joints have a higher corrosion potential and lower corrosion current density than SMA490BW steel. These data suggest that the rust layers formed on the welded joints are more protective to the substrate.

**Table 4.** Electrochemical parameters obtained from the polarization curve of SMA490BW steel and its welded joints.

Corrosion Time	SMA490BW		Welded Joints	
	$E_{\text{corr}}(\text{V/SCE})$	$i_{\text{corr}}(\times 10^{-5} \text{A/cm}^2)$	$E_{\text{corr}}(\text{V/SCE})$	$i_{\text{corr}}(\times 10^{-5} \text{A/cm}^2)$
75 h	−0.553	1.749	−0.489	1.654
100 h	−0.644	1.411	−0.635	1.393
125 h	−0.716	1.187	−0.698	1.135
150 h	−0.806	1.063	−0.782	0.962

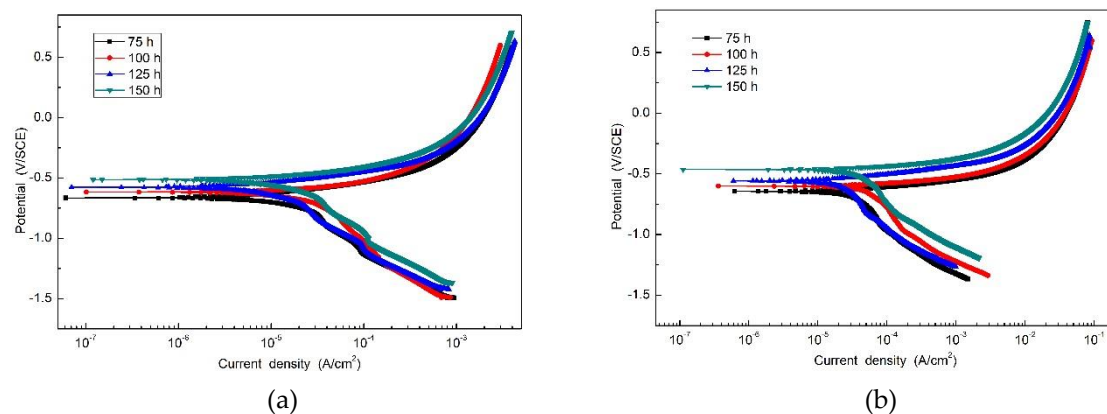
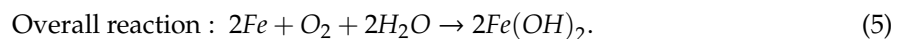
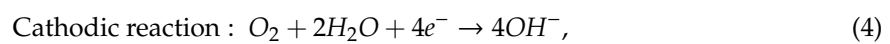
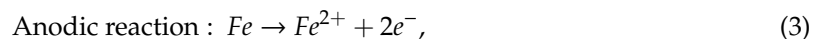


**Figure 7.** Potentiodynamic polarization curve of (a) SMA490BW steel and (b) welded joints after the periodic immersion wet/dry cyclic corrosion test.

### 3.4. Corrosion Mechanism

The atmospheric corrosion of metal is an electrochemical corrosion process that occurs in the thin liquid film in nature. Under conditions of the periodic immersion wet/dry cyclic corrosion test, the surfaces of SMA490BW steel and its welded joints soon lose their metallic luster and begin to corrode. In the wet stage with the presence of oxygen, the anodic oxidation and cathodic reduction reactions in the electrochemical process happen as follows [26]:



$Fe(OH)_2$ , which is a transient product in the rust, is oxidized to form much amorphous oxide (ferric and ferrous) and  $Fe(OH)_3$  immediately in the dry stage. Then,  $\gamma$ - $FeOOH$  is formed by crystallization of the amorphous oxide, and transforms afterward to  $\alpha$ - $FeOOH$  or  $Fe_3O_4$ . It is recognized that  $SO_2$  has the worst effect among air pollutants. A part of  $SO_2$  adsorbs onto the surface of steel leading to the presence of diffluent  $FeSO_4$ , which is obtained by the chemical reaction between  $SO_2$ ,  $O_2$ , and  $Fe$ . Furthermore,  $H_2SO_4$  is obtained by the further oxidation and strong hydrolysis of  $FeSO_4$ , and then  $H_2SO_4$  reacts with  $Fe$  [27,28]. For steel, this whole process keeps recurring due to autocatalysis so that much rust is generated from a molecule of  $SO_2$ . In this way, the rusting process is greatly accelerated. However, the corrosion resistance of SMA490BW steel and its welded joints is enhanced due to the addition of alloy elements, such as Ni and Cr. During the early corrosion period, some  $Ni^{2+}$  ions replace  $Fe^{2+}$  ions, and nanoscale  $Fe_2NiO_4$  separates out. Thus, nanoscale  $Fe_2NiO_4$  offers enough nucleation centers for the formation of nano-reticular  $Fe(O,OH)_6$  and inhibits its growth [29,30]. For this reason, a compact, refined and ion-selective rust layer is easy to form. Although corrosion resistance is enhanced with increasing Ni content, there is still a threshold value. Cr can infinitely dissolve in Fe solution so that some  $Cr^{2+}$  ions replace  $Fe^{2+}$  ions, and this leads to the formation of  $Cr_xFe_{1-x}OOH$  [31]. The rust layers become ion selective due to  $Cr_xFe_{1-x}OOH$  and prevent sulfate ions from permeating effectively [32–34]. Furthermore, the enrichment of Cr in defects and grain boundaries has a positive effect on the formation of more compact rust layers. Consequently, the alloy elements have a direct influence on the corrosion resistance of SMA490BW steel and its welded joints.

To explain the difference of corrosion resistance, the main chemical composition of SMA490BW steel and its welded joints before and after the periodic immersion wet/dry cyclic corrosion test were analyzed by EDS and are given in Table 5. Compared with SMA490BW steel, the content of Ni as well as the content of Cr in the welded joints are higher because of the welding wire with a higher content of Ni and Cr. Moreover, the rust layers of the welded joints after 150 h still have a higher content of

Ni and Cr than that of SMA490BW steel. As mentioned above, Ni and Cr elements have a positive effect on enhancing corrosion resistance. Therefore, the automatic MAG welded joints exhibit better corrosion resistance than SMA490BW steel because of the higher content of alloy elements.

**Table 5.** Main chemical composition of SMA490BW steel and its welded joints before and after the periodic immersion wet/dry cyclic corrosion test (wt %).

Materials	Fe	O	Ni	Cu	Cr	S
SMA490BW (before)	92.9	-	0.25	0.32	0.54	-
SMA490BW (after)	58.51	34.95	0.17	0.15	1.26	1.39
Welded joints (before)	89.94	-	0.50	0.36	0.75	-
Welded joints (after)	56.21	36.21	0.29	0.22	1.81	1.04

#### 4. Conclusions

The corrosion behavior of SMA490BW steel and its welded joints used for high-speed train bogies was investigated using the periodic immersion wet/dry cyclic corrosion test to simulate an industrial atmospheric environment. The main results are as follows.

The corrosion weight loss rate of SMA490BW steel and its welded joints decreases with increasing corrosion time and then becomes stable because the rust layers after 150 h have a good effect on protecting the substrate.

The alloy elements Ni and Cr accelerate the formation of protective rust layers and are beneficial in enhancing corrosion resistance.

The corrosion weight loss rate, XRD results, SEM micrographs, EDS results, thickness of rust layers, and electrochemical parameters indicate that the welded joints have a better corrosion resistance compared with SMA490BW steel in a simulated industrial atmospheric environment. The main reason is that the content of Ni and Cr in the welded joints is higher than that in SMA490BW steel.

**Author Contributions:** Methodology, X.W., C.S., S.H.; Investigation, S.H., W.Q., Z.Z., R.T.; Data processing, S.H.; all the authors contributed to writing the original draft of the paper. Writing—review and editing, S.H.

**Funding:** This work was supported by the National Natural Science Foundation of China (No. 51605070).

**Conflicts of Interest:** The authors declare no conflict of interest.

#### References

- Lu, Y.; Xiang, P.; Dong, P.; Zhang, X.; Zeng, J. Analysis of the effects of vibration modes on fatigue damage in high-speed train bogie frames. *Eng. Fail. Anal.* **2018**, *89*, 222–241. [[CrossRef](#)]
- Liu, Y.; Wang, L.; Chou, K. Effects of cerium on resistance to pitting corrosion of spring steel used in fasteners of high-speed railway. *Steel Res. Int.* **2014**, *85*, 1510–1516. [[CrossRef](#)]
- Shi, S.; Su, C. Corrosion inhibition of high speed steel by biopolymer HPMC derivatives. *Materials* **2016**, *9*, 612. [[CrossRef](#)] [[PubMed](#)]
- Shen, L.; Chen, H.; Che, X.; Xu, L. Corrosion-fatigue crack propagation of aluminum alloys for high-speed trains. *Int. J. Mod. Phys. B* **2017**, *31*, 1744009. [[CrossRef](#)]
- Chen, X.; Dong, J.; Han, E.; Ke, W. Effect of Ni on the ion-selectivity of rust layer on low alloy steel. *Mater. Lett.* **2007**, *61*, 4050–4053. [[CrossRef](#)]
- Cheng, X.; Tian, Y.; Li, X.; Zhou, C. Corrosion behavior of nickel-containing weathering steel in simulated marine atmospheric environment. *Mater. Corros.* **2014**, *65*, 1033–1037. [[CrossRef](#)]
- Hao, L.; Zhang, S.; Dong, J.; Ke, W. Atmospheric corrosion resistance of MnCuP weathering steel in simulated environments. *Corros. Sci.* **2011**, *53*, 4187–4192. [[CrossRef](#)]
- Zhu, T.; Huang, F.; Liu, J.; Hu, Q.; Li, W. Effects of inclusion on corrosion resistance of weathering steel in simulated industrial atmosphere. *Anti. Corros. Method. Mater.* **2016**, *63*, 490–498. [[CrossRef](#)]
- He, B.; Xiong, L.; Jiang, M.; Li, L. Surface grain refinement mechanism of SMA490BW steel cross joints by ultrasonic impact treatment. *Int. J. Min. Met. Mater.* **2017**, *4*, 60–64. [[CrossRef](#)]

10. Ma, Y.; Li, Y.; Wang, F. Corrosion of low carbon steel in atmospheric environments of different chloride content. *Corros. Sci.* **2009**, *51*, 997–1006. [[CrossRef](#)]
11. Wang, Z.; Liu, J.; Wu, L.; Han, R.; Sun, Y. Study of the corrosion behavior of weathering steels in atmospheric environments. *Corros. Sci.* **2013**, *67*, 1–10. [[CrossRef](#)]
12. Sugimoto, I.; Kita, K. Evaluation of applicability for Ni-advanced weathering steels and bridge high-performance steels to railway steel bridges. *Quart. Rep. Railw. Tech. Res. Inst. Jpn.* **2010**, *51*, 33–37. [[CrossRef](#)]
13. Chen, Y.; Tzeng, H.; Wei, L.; Wang, L.; Oung, J.; Shih, H. Corrosion resistance and mechanical properties of low-alloy steels under atmospheric conditions. *Corros. Sci.* **2005**, *47*, 1001–1021. [[CrossRef](#)]
14. Fuente, D.; Díaz, I.; Simancas, J.; Chico, B.; Morcillo, M. Long-term atmospheric corrosion of mild steel. *Corros. Sci.* **2011**, *23*, 604–617. [[CrossRef](#)]
15. Diaz, I.; Cano, H.; Fuente, D.; Chico, B.; Vega, J.; Morcillo, M. Atmospheric corrosion of Ni-advanced weathering steels in marine atmospheres of moderate salinity. *Corros. Sci.* **2013**, *76*, 348–360. [[CrossRef](#)]
16. Guo, M.; Pan, C.; Wang, Z.; Han, W. A study on the initial corrosion behavior of carbon steel exposed to a simulated coastal-industrial atmosphere. *Acta Metall. Sin.* **2018**, *54*, 65–75.
17. Wang, Z.; Li, P.; Guan, Y.; Chen, Q.; Pu, S. The corrosion resistance of ultralow carbon bainitic steel. *Corros. Sci.* **2009**, *51*, 954–961. [[CrossRef](#)]
18. Guo, J.; Yang, S.; Shang, C.; Wang, Y.; He, X. Influence of carbon content and microstructure on corrosion behavior of low alloy steels in a Cl<sup>-</sup> containing environment. *Corros. Sci.* **2008**, *51*, 242–251. [[CrossRef](#)]
19. Tanaka, H.; Mishima, R.; Hatanaka, N.; Ishikawa, T.; Nakayama, T. Formation of magnetite rust particles by reacting iron powder with artificial  $\alpha$ -,  $\beta$ - and  $\gamma$ -FeOOH in aqueous media. *Corros. Sci.* **2014**, *78*, 384–387. [[CrossRef](#)]
20. Mi, F.; Wang, X.; Liu, Z.; Wang, B.; Peng, Y.; Tao, D. Industrial atmospheric corrosion resistance of P-RE weathering steel. *J. Iron. Steel Res. Int.* **2011**, *18*, 67–73. [[CrossRef](#)]
21. Pan, C.; Han, W.; Wang, Z.; Wang, C.; Yu, G. Evolution of initial atmospheric corrosion of carbon steel in an industrial atmosphere. *J. Mater. Eng. Perform.* **2016**, *25*, 5382–5390. [[CrossRef](#)]
22. Antony, H.; Perrin, S.; Dillmann, P.; Legrand, L.; Chausse, A. Electrochemical study of indoor atmospheric corrosion layers formed on ancient iron artefacts. *Electr. Acta* **2007**, *52*, 7754–7759. [[CrossRef](#)]
23. Kamimura, T.; Hara, S.; Miyuki, H.; Yamashita, M.; Uchida, H. Composition and protective ability of rust layer formed on weathering steel exposed to various environments. *Corros. Sci.* **2006**, *48*, 2799–2812. [[CrossRef](#)]
24. Ma, Y.; Li, Y.; Wang, F. The atmospheric corrosion kinetics of low carbon steel in a tropical marine environment. *Corros. Sci.* **2010**, *52*, 1796–1800. [[CrossRef](#)]
25. Li, Y.; Cheng, Y. Effect of surface finishing on early-stage corrosion of a carbon steel studied by electrochemical and atomic force microscope characterizations. *Appl. Surf. Sci.* **2016**, *366*, 95–103. [[CrossRef](#)]
26. Qian, Y.; Ma, C.; Niu, D.; Xu, J.; Li, M. Influence of alloyed chromium on the atmospheric corrosion resistance of weathering steels. *Corros. Sci.* **2013**, *74*, 424–429. [[CrossRef](#)]
27. Tamura, H. The role of rusts in corrosion and corrosion protection of iron and steel. *Corros. Sci.* **2008**, *50*, 1872–1883. [[CrossRef](#)]
28. Martínez, C.; Briones, F.; Villarroel, M.; Vera, R. Effect of Atmospheric Corrosion on the Mechanical Properties of SAE 1020 Structural Steel. *Materials* **2018**, *11*, 591. [[CrossRef](#)]
29. Kimura, M.; Suzuki, T.; Shigesato, G.; Kihira, H.; Tanabe, K. Fe(O,OH)<sub>6</sub> network structure of rust formed on weathering steel surfaces and its relationship with corrosion resistance. *Nippon. Steel Tech. Rep.* **2003**, *87*, 17–20.
30. Nishimura, T.; Katayama, H.; Noda, K.; Kodama, T. Effect of Co and Ni on the corrosion behavior of low alloy steels in wet/dry environments. *Corros. Sci.* **2000**, *42*, 1611–1621. [[CrossRef](#)]
31. Yamashita, M.; Miyuki, H.; Matsuda, Y.; Magano, H.; Misawa, T. The long term growth of the protective rust layer formed on weathering steel by atmospheric corrosion during a quarter of a century. *Corros. Sci.* **1994**, *36*, 283–299. [[CrossRef](#)]
32. Xiao, X.; Peng, Y.; Ma, C.; Tian, Z. Effects of alloy element and microstructure on corrosion resistant property of deposited metals of weathering steel. *J. Iron Steel Res. Int.* **2016**, *23*, 171–177. [[CrossRef](#)]
33. Townsend, H. Effects of alloying elements on the corrosion of steel in industrial atmospheres. *Corrosion* **2001**, *57*, 497–501. [[CrossRef](#)]

34. Zhang, H.; Zhao, X.; Xu, D.; Liu, Y.; Qiu, X. New insight into high frequency impacting and rolling of 2A12 aluminum welded joint involving nanocrystallization. *Appl. Surf. Sci.* **2019**, *488*, 115–127. [[CrossRef](#)]



© 2019 by the authors. Licensee MDPI, Basel, Switzerland. This article is an open access article distributed under the terms and conditions of the Creative Commons Attribution (CC BY) license (<http://creativecommons.org/licenses/by/4.0/>).